

Evidence of a Shockley-Read-Hall Defect State Independent of Band-Edge Energy in InAs/In(As,Sb) Type-II Superlattices

Y. Aytac,^{1,*} B. V. Olson,² J. K. Kim,² E. A. Shaner,² S. D. Hawkins,² J. F. Klem,² M. E. Flatté,¹ and T. F. Bogess¹

¹*Department of Physics and Astronomy and Optical Science and Technology Center, University of Iowa, Iowa City, Iowa 52242, USA*

²*Sandia National Laboratories, Albuquerque, New Mexico 87185, USA*

(Received 29 January 2016; revised manuscript received 5 February 2016; published 24 May 2016)

A set of seven InAs/In(As, Sb) type-II superlattices (T2SLs) are designed to have specific band-gap energies between 290 meV (4.3 μm) and 135 meV (9.2 μm) in order to study the effects of the T2SL band-gap energy on the minority-carrier lifetime. A temperature-dependent optical pump-probe technique is used to measure the carrier lifetimes, and the effect of a midgap defect level on the carrier-recombination dynamics is reported. The Shockley-Read-Hall (SRH) defect state is found to be at energy of approximately -250 ± 12 meV relative to the valence-band edge of bulk GaSb for the entire set of T2SL structures, even though the T2SL valence-band edge shifts by 155 meV on the same scale. These results indicate that the SRH defect state in InAs/In(As, Sb) T2SLs is singular and is nearly independent of the exact position of the T2SL band-gap or band-edge energies. They also suggest the possibility of engineering the T2SL structure such that the SRH state is removed completely from the band gap, a result that should significantly increase the minority-carrier lifetime.

DOI: 10.1103/PhysRevApplied.5.054016

I. INTRODUCTION

InAs/In(As, Sb) type-II superlattices (T2SLs) were proposed as an alternative material to Hg(Cd,Te) for infrared (IR) detection in 1985 [1]. Since then, many different designs and growth methods have been studied to improve the structural and optical properties of these T2SLs to realize next-generation IR detectors and focal plane arrays [2–11]. Improvements in detectivity and responsivity have been the main focus of T2SL photodetector development; however Hg(Cd,Te) continues to set the goals for dark current and sensitivity [12]. Improvements in T2SL detector performance depend critically on the minority-carrier (MC) lifetime, which currently is controlled by flaw-related Shockley-Read-Hall (SRH) recombination [5,6,8–10,13] at typical operating temperatures. Previously, InAs/In(As, Sb) T2SLs have been shown to have MC lifetimes of approximately 10 μs in the midwave infrared (MWIR) [6,13] and hundreds of nanoseconds in the long-wave infrared (LWIR) [14,15], with Auger coefficients reported between 1 and 5×10^{-26} cm^6/s for MWIR [6,10] and low 10^{-25} cm^6/s for LWIR [15]. These results indicate that InAs/In(As, Sb) T2SLs are prime candidates for next-generation IR detectors.

Temperature- and carrier-density-dependent studies on MWIR InAs/In(As, Sb) T2SLs have shown that SRH recombination limits the MC carrier lifetime at low temperatures and low-injection carrier densities [5,6,8–10,13]. The mid-band-gap SRH recombination centers identified in MWIR InAs/In(As, Sb) T2SLs have been previously

reported to be at an energy approximately 250 meV below the valence-band edge of bulk GaSb [5,9]. One significant benefit of superlattice (SL) structures is that the position of the SL valence-band- (VB) and conduction-band- (CB) edge energies and, hence, the SL band gap (E_g), on an absolute energy scale is determined by the layer thicknesses, compositions, and specific materials that make up the structure and can, therefore, be engineered. Recently, a method that utilizes this flexibility inherent to SL structures has been proposed to mitigate the effects of parasitic SRH recombination centers [16]. Essentially, if a mid-band-gap SRH defect is identified, the SL structure may be engineered such that the position of the SL band gap on an absolute energy scale is shifted relative to the SRH defect. If this shift in SL band-gap position is on the order of $1/2 E_g$, the SRH defect state will then be near a SL band edge, or even within the valence or conduction bands, and rendered ineffective as a recombination center as in Fig. 1. This method, of course, assumes that the SRH defect state does not float with the T2SL band-edge energies but instead has an energy determined by the work function of the material-specific defect. For InAs/In(As, Sb) T2SLs, this strategy involves engineering the SL structure using the layer thicknesses of InAs and In(As,Sb) and the alloy composition to shift the T2SL band-edge energies in absolute energy. A previous study that focused on engineering the InAs/In(As, Sb) structure, while keeping a constant band gap near 5.2 μm , showed that an approximately $2k_B T$ energy shift in the T2SL VB energy is possible, which caused the MC lifetime to increase from approximately 3 to 6 μs [9]. This result demonstrates the feasibility of

*yigit-aytac@uiowa.edu

modifying the SRH lifetime through band-structure engineering. A larger modification of the T2SL band-gap position is required, however, to fully remove the SRH defect from the band gap and realize significantly longer MC lifetimes in this material system.

Here, time-resolved and temperature-dependent differential-transmission measurements and a MC lifetime analysis [5,9] are used to determine the SRH defect-energy level in a series of seven InAs/InAs_{1-x}Sb_x T2SL samples engineered to have different absolute T2SL valence-band energies. The MC lifetimes, which include contributions from SRH, radiative, and Auger recombination, are observed to be strongly correlated with the T2SL band-edge energies and the SRH defect energy. This SRH defect is found to be near mid-band-gap for the MWIR samples and transitions to a shallow defect state for the LWIR samples.

II. EXPERIMENTAL RESULTS

Samples are grown by molecular beam epitaxy using previously described techniques [6,9,10,13]. For all seven samples, the epitaxial layers consist of a GaSb buffer layer, a bottom 100-nm Al(As,Sb) barrier layer, an unintentionally doped and nominally 4- μ m-thick T2SL absorber layer, a top 100-nm Al(As,Sb) barrier layer, and a 150-nm In(As,Sb) cap layer. Photoluminescence (PL) spectra at

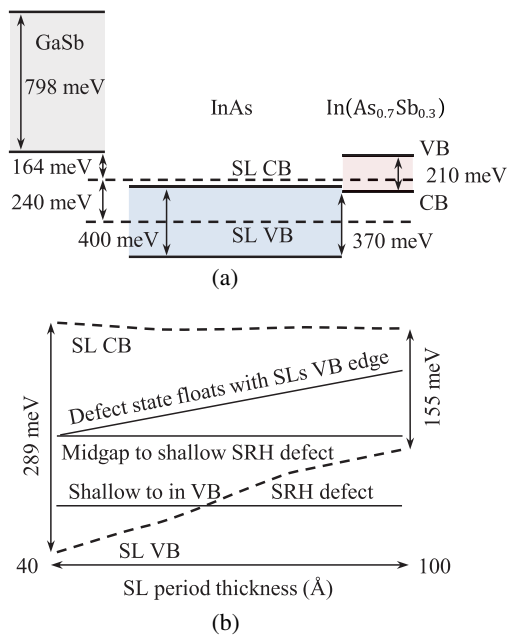


FIG. 1. (a) Relative positions of the CB- and VB-edge energies for bulk GaSb, InAs, and In(As_{0.7}Sb_{0.3}) (solid lines), where InAs and In(As_{0.7}Sb_{0.3}) are strained to GaSb. The dashed lines in (a) correspond to the SL band-edge energies of a strain-balanced 45.8-Å InAs/15.0-Å In(As_{0.7}Sb_{0.3}) SL. (b) Strain-balanced InAs/In(As_{0.7}Sb_{0.3}) SL band-edge energies as a function of SL period thickness on an absolute energy scale. The solid curves in (b) correspond to three possible trends in recombination-center energy level as the SL band edges are shifted in energy.

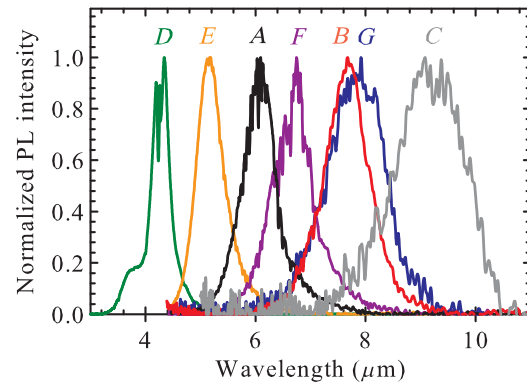


FIG. 2. Normalized photoluminescence spectra of the seven InAs/In(As,Sb) T2SL samples at 80 K.

80 K are plotted in Fig. 2 for the seven samples showing the shifts in T2SL band-gap energy as the layer thicknesses and alloy composition are varied. The T2SL layer structures determined using high-resolution x-ray diffraction (HRXRD) measurements are listed in Table I. Both the HRXRD and PL measurements confirm the designed layer structure and T2SL band-gap energies. In addition, capacitance-voltage measurements of these samples are used to determine the equilibrium carrier density (in this case, the majority-carrier electron concentrations, n_0) of the T2SLs, and the results are also listed in Table I [9,10,17]. A 14-band $\mathbf{k} \cdot \mathbf{p}$ model [18] is used to calculate other pertinent electronic and optical properties of the as-grown T2SL structures, with the information compiled in Table I.

The time-resolved pump-probe technique utilizes a tunable subpicosecond MWIR pump laser for excitation, and a pulsed quantum cascade laser probe that is electronically synchronized to the pump laser. A precision electronic delay line provides a variable delay between the approximately 100-fs pump and approximately 3-ns duration, 9.3- μ m wavelength probe, and differential transmission ($\Delta T/T$) measurements are used to investigate the nonequilibrium carrier-recombination dynamics of the T2SLs at temperatures between 77 and 293 K [5,6,9,13]. For the measurements reported here, the pump and probe beams have radii (e^{-1} of the intensity) of approximately 1100 and 200 μ m, respectively. A pump wavelength of 3.55 μ m (350 meV) is used, and the initial optically injected excess carrier densities are calculated using the measured incident pump pulse energy, pump spot size at the sample, the absorption coefficient obtained from the 14 band $\mathbf{k} \cdot \mathbf{p}$ model, and taking into account losses due to optical windows and Fresnel reflections.

Minority-carrier lifetimes are measured using the time-resolved $\Delta T/T$ data in a manner discussed previously, and we refer the reader to Refs. [5,9,13] for more details on these measurements. In this analysis, the density-dependent carrier-recombination rate data, at a specific temperature, are fit to the model which includes the SRH, radiative, and Auger recombination terms [5,9,19,20]. The MC lifetime

TABLE I. Summary of the physical properties of the seven InAs/In(As,Sb) T2SL structures. The layer thicknesses and In(As,Sb) compositions are determined from high-resolution x-ray diffraction. The T2SL band-gap energies (E_g) are determined from 80-K photoluminescence spectra measurements. The T2SL conduction-band- (E_c), valence-band- (E_v) edge energies, and absorption coefficients are obtained using a 14-band $\mathbf{k} \cdot \mathbf{p}$ model. The band-edge energies are listed relative to the valence-band edge of bulk GaSb.

Sample ID	InAs/InAs _{1-x} Sb _x thickness (Å)	X (%)	No. of SL periods	n_0 (cm ⁻³)	E_g (meV)	E_v (meV)	E_c (meV)	α (cm ⁻¹)
A	57.7/13.1	38 ± 2	580	7.6 × 10 ¹⁴	203.9	-370.0	-167.0	3203
B	72.2/16.1	39 ± 2	460	9.7 × 10 ¹⁴	161.6	-328.9	-167.0	2257
C	85.6/19.1	39 ± 2	380	7.2 × 10 ¹⁴	134.5	-304.0	-170.0	2467
D	30.1/9.8	31 ± 2	990	6.7 × 10 ¹⁴	289.6	-445.0	-155.0	3387
E	45.8/15.0	30 ± 2	660	4.5 × 10 ¹⁴	240.2	-403.0	-164.0	3526
F	61.9/20.2	31 ± 2	500	5.7 × 10 ¹⁴	185.2	-346.0	-161.0	2844
G	76.5/25.0	30 ± 2	400	6.5 × 10 ¹⁴	155.2	-317.0	-226.0	2534

is then determined using the recombination rate expression including the individual contributions of these three main recombination rates in their low-level injection forms. The MC lifetime values at each measured temperature are fit to the lifetime models for the low excess carrier density limit where the defect-energy level E_t , capture cross section and defect density values σN_t , and the Block overlap constant $|F_1 F_2|$ [5,14] are used as fitting parameters. Note that a single defect state is sufficient for fitting the temperature-dependent MC lifetime. The resulting MC lifetime data for samples A-G are shown in Fig. 3, where the data are analyzed taking into account SRH, radiative, and Auger recombination [5,9,10]. Because of the distinctive dependence that each of these three carrier-recombination mechanisms have on the excess carrier density (Δn), n_0 , and temperature (T), the recombination mechanisms that are limiting the MC lifetime can be uniquely identified [5,9,10].

III. DISCUSSION

Previous reports identify that SRH recombination is the mechanism limiting the MC lifetimes in both MWIR and LWIR unintentionally doped InAs/In(As, Sb) T2SLs and In(As,Sb) alloys at temperatures relevant to photodetector operation [2,5,9,10,19–22]. The carrier lifetime associated with low-injection-level SRH recombination for a single-defect level is expressed as [19,20,23]

$$\tau_{\text{SRH}} = \frac{\tau_{pO}(n_0 + n_1) + \tau_{nO}(p_0 + p_1)}{n_0 + p_0} \quad (1)$$

where τ_{pO} and τ_{nO} are the defect capture time constants for electrons and holes, n_0 and p_0 are the equilibrium densities of electrons and holes, respectively, and

$$n_1 = N_c \exp\left[\frac{(E_t - E_c)}{k_B T}\right], \quad p_1 = N_v \exp\left[\frac{(E_v - E_t)}{k_B T}\right], \quad (2)$$

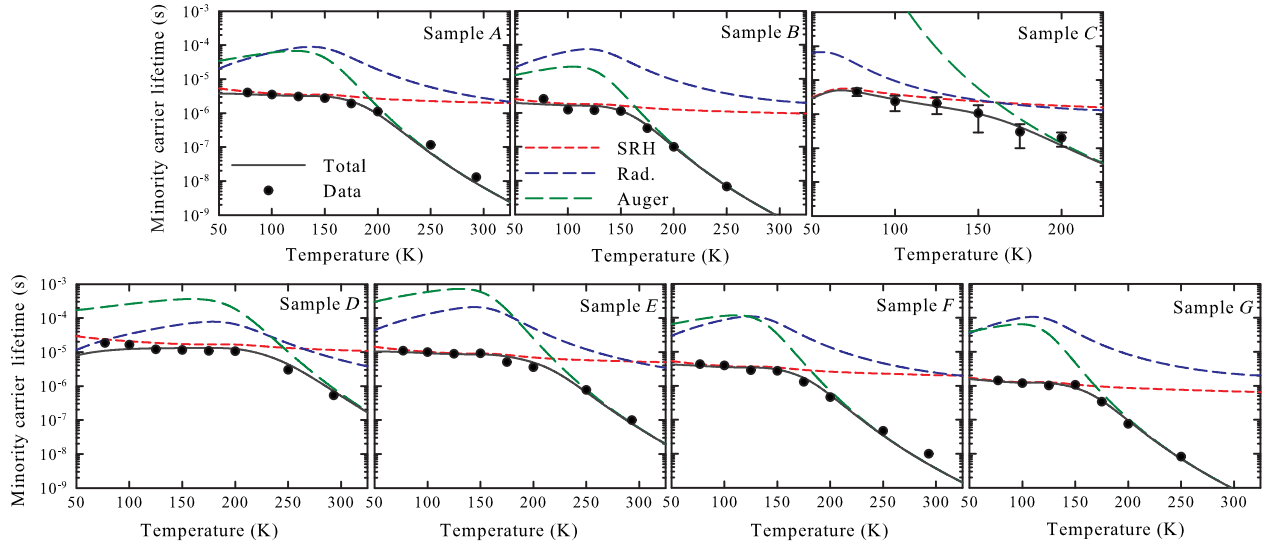


FIG. 3. MC lifetime results as a function of temperature for the seven InAs/In(As,Sb) type-II superlattice samples. The solid black curves are the best fits to the measured data and represent the total MC lifetime. The red, blue, and green dashed curves are the deconvoluted low-level injection contributions of SRH, radiative, and Auger recombination to this total lifetime, respectively.

where k_B is the Boltzmann constant, E_c and E_v are the T2SL conduction-band- and valence-band-edge-energies, respectively, and E_t is the SRH defect energy. Here, N_v and N_c are the effective conduction- and valence-band density of states in a three-dimensional approximation [19,20,23]. The capture time constants τ_{pO} and τ_{nO} are proportional to the inverse product of the defect concentration N_t and the capture cross sections σ_n and σ_p for electrons and holes, respectively, as

$$\tau_{pO} = (N_t \sigma_p v_p)^{-1}, \quad \tau_{nO} = (N_t \sigma_n v_n)^{-1}, \quad (3)$$

where v_n and v_p are electron and hole thermal velocities, respectively. The temperature-dependent behavior of the SRH expression is illustrated in Fig. 4 for sample A. The SRH defect state is more efficient as a recombination center when it is near the mid-band-gap, resulting in shorter SRH lifetimes as shown in Fig. 4(a). On the other hand, if the SRH defect state is instead closer to the VB edge (or CB edge), the SRH defect is less efficient, resulting in a longer SRH lifetime. In the first region (I) in Fig. 4(b), the SRH lifetime is limited by the capture of minority carriers and $\tau_{\text{SRH}}^{\text{I}} \rightarrow \tau_{pO}$. The SRH lifetime scales as $T^{-1/2}$ in this temperature range. The doping level (n_0) determines the onset position of the increased SRH lifetime in the temperature regime where SRH recombination is least efficient. For example, in region (II), the SRH lifetime increases exponentially as $\tau_{\text{SRH}}^{\text{II}} \rightarrow [(N_c)/(\tau_{pO} n_0)] \text{Exp}(-E_t/k_B T)$, where the onset of this increase is determined by n_0 . At

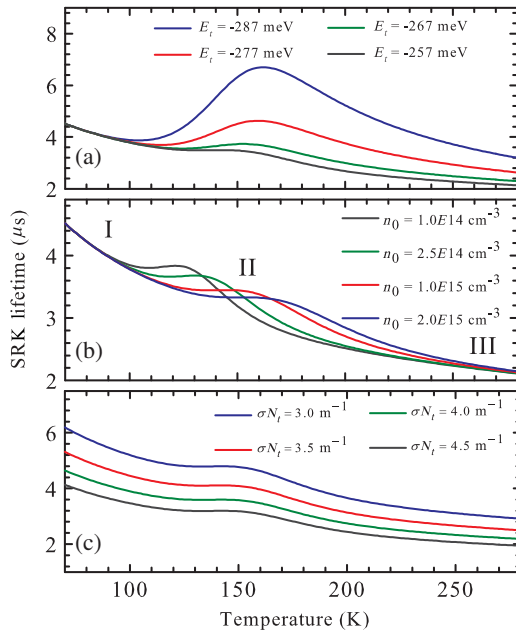


FIG. 4. Influence of (a) SRH defect energy, (b) equilibrium carrier density, and (c) capture probability on the SRH lifetime is shown for the sample A under low-level-injection conditions. In each case, all other parameters are held constant while the specified values are varied.

higher temperatures (region III), where the $n_0 = p_0 = n_i$ condition is fulfilled, the SRH lifetime decreases exponentially due to increasing equilibrium carrier density and temperature. This is the intrinsic regime. The capture probability defined as σN_t acts as a scaling factor that primarily provides a vertical shift of the SRH lifetime at a particular temperature rather than a change in the overall temperature dependence (or shape as a function of temperature) as shown in Fig. 4(c). Notice that E_t and σN_t are used as temperature-independent fitting parameters in the analysis presented here. With these dependences on temperature, the SRH defect energy can be uniquely identified based on the overall trend that the SRH-limited MC lifetime has with temperature, while the magnitude is primarily determined by σN_t . Under the assumption of a static SRH defect, there are two possible interpretations of the measured MC lifetimes. First, the SRH defect state shifts from a deep to shallow level due to the engineered shifts in T2SL valence-band-edge energies, and the SRH lifetime is correspondingly affected as expressed previously. Second, the SRH defect-energy level is near mid-band-gap for each sample, and the variation in MC lifetimes is due instead to different SRH trap densities affecting τ_{pO} and τ_{nO} . Since all samples have similar MBE growth parameters, the SRH defect density N_t should not vary significantly from sample to sample. However, the cross section of carriers can vary with engineered layer thickness and band-gap value which can change the total capture probability. The best-fit parameters are listed in Table II, where the reported uncertainties are calculated by analyzing the Hessian matrices from the lifetime model results. In order to minimize the error attached to the extracted SRH defect energies, the SRH lifetime must dominate the MC lifetime over a broad range of temperatures. In addition, the Auger lifetime fitting parameter $|F_1 F_2|$ is also extracted from temperature-dependent MC lifetime data analysis, the results of which are shown in Table II.

Samples A, B, and C corresponding to Sb mole fractions of approximately 40% in the alloy layer are engineered to step the T2SL valence-band edge with a VB shift of

TABLE II. Summary the SRH defect energy E_t , capture probability σN_t , and Auger recombination Bloch function overlap parameter $|F_1 F_2|$ determined from the temperature-dependent minority-carrier-lifetime fitting. Defect-energy levels are reported relative to the valence-band edge of bulk GaSb.

Sample ID	E_t (meV)	σN_t (m^{-1})	$ F_1 F_2 $
A	-248 ± 8	4.1 ± 0.3	0.16
B	-230 ± 16	8.2 ± 2	0.15
C	-275 ± 5	10.8 ± 6	0.06
D	-280 ± 30	0.4 ± 0.17	0.12
E	-260 ± 10	1.9 ± 0.15	0.14
F	-235 ± 8	4.0 ± 0.13	0.14
G	-225 ± 10	12.1 ± 0.9	0.13

approximately 70 meV. The MC lifetimes are correspondingly observed to be approximately 4, 2, and 4.6 μs at 77 K for samples *A*, *B*, and *C*, respectively. The substantially long MC lifetime in sample *C*, despite its comparatively small band-gap energy, is attributed to the SRH defect being shifted closer to the T2SL valence-band edge; in fact, it is found to be approximately 70 meV closer than sample *B* and approximately 93 meV closer than sample *A* as shown in Fig. 5. The 93-meV shift in the SRH defect energy is significantly larger than the T2SL VB shift of 70 meV realized in this series of samples. While some variation in the extracted SRH defect energy is found, this variation is relatively small compared to the sample-to-sample variation in the valence-band edge. We, therefore, consider the SRH defect energy in the InAs/In(As,Sb) T2SLs is at approximately -250 meV below the VB edge of GaSb. Notice that the σN_t value also increases gradually with decreasing band gap (as seen by the listed values in Table II), which corresponds to a decreasing SRH lifetime. It is, therefore, unlikely that the observed trends in the MC lifetimes are due to simply differences in capture cross section, since this requires σN_t to decrease from samples *A* to *C* to account for the long MC lifetimes. Samples *D* to *G*, which have Sb mole compositions of 30%, are similarly engineered to step the T2SL VB edge, with the resulting as-grown structures realizing an approximately 128-meV shift in the T2SL VB edge. The CB edge shifts less than 10 meV. Therefore, the defect energy is, thus, engineered to shift relatively closer to the T2SL VB edge for samples *D* through *G*, as shown in Fig. 5. The SRH defect energy is found again to be approximately 250 meV below the GaSb VB edge for these four samples. Even though the VB edge shifts towards the SRH defect state and the SRH defect energy is quite shallow, we still find that the MC lifetime is limited by SRH recombination for the sample *G*. The extracted capture probability values increase gradually from sample *D* to *G* but again cannot account for the observed trends in MC lifetime. A change in the SRH defect energy relative to the T2SL band-edge energies is required to fully describe the

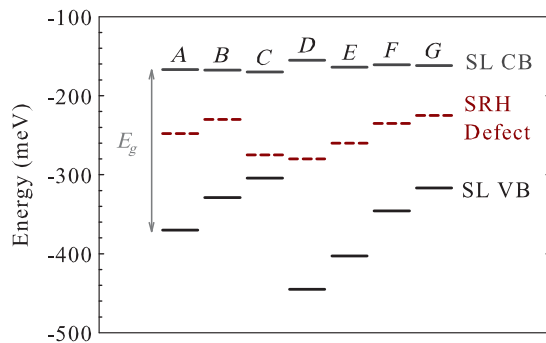


FIG. 5. VB- and CB-edge energies for the InAs/In(As,Sb) T2SL series (samples *A* through *G*). The measured SRH defect-energy levels are also plotted as the dashed lines. The VB edge of bulk GaSb is taken as zero energy on this scale.

results presented here. Overall, the SRH defect state is found to be at an energy of 250 ± 12 meV for the seven samples, as shown in Fig. 5, determined from an average of the extracted SRH defect energies.

In group III-V semiconductors, the vacancies, antisites, and interstitial defects are the most common point defects. Density-functional-theory calculations [24] indicate that the vacancy of In atoms produces a p -like T_2 -symmetry state approximately 100 meV below the conduction-band edge of InAs. In tensile strain, this vacancy-state energy is located 37 meV below the strained InAs conduction-band edge, which is within 3 meV of the SRH recombination center energy reported here. Antisites occur in binary alloys when the electronegativity and size between two constituent atoms are small. In InAs binary alloy, it forms as the antibonding A_1 state and is about 30 meV below the conduction-band edge of InAs which holds the same position in strain. This state is within 4 meV of the reported SRH recombination energy. Between these two types of point defects, the antisites are more common in binary alloys, which is most probably associated with the InAs region and registered to the (strained) bulk constituent. The Sb_{As} replacement related to the Sb diffusion at the SL interfaces can cause localized defect states; however, the energy level of these antisites is more than an electronvolt below the InAs valence-band edge [25].

IV. SUMMARY

In summary, time-resolved MC lifetime measurements are used to investigate the nonequilibrium carrier-recombination dynamics in a series of band-structure-engineered InAs/In(As,Sb) T2SLs. The T2SL structures are designed such that their VB edges display significant shifts in absolute energy, while the conduction-band edges remain comparatively fixed. The carrier-lifetime measurements indicate that the MC lifetime is limited by SRH recombination for all the samples at temperatures below approximately 175 K, which allows extraction of the SRH defect-energy levels. The defect-energy levels provide evidence that the SRH recombination center in InAs/In(As,Sb) T2SLs is singular in nature, and its energy position is nominally independent of the T2SL structure. Analysis of the MC lifetime data suggests that this parasitic SRH defect state is at an average energy of 250 ± 12 meV below the VB edge of bulk GaSb. These results provide compelling evidence that the minority-carrier lifetime in InAs/In(As,Sb) T2SLs can be substantially altered by engineering the electronic band structure. For instance, a T2SL sample with a band gap of 134 meV (approximately 9.2- μm wavelength) is observed to have a MC lifetime of 4.6 μs at a temperature of 77 K. This enhanced SRH lifetime is a direct consequence of the T2SL structure being engineered such that the T2SL VB edge is shifted up in energy, effectively shifting the SRH defect state away from mid-band-gap and closer to the VB edge. It is likely that

significant improvement to the carrier lifetime in InAs/In(As, Sb) T2SLs can be achieved through electronic band engineering of the T2SL structure to render parasitic defect states ineffective as SRH recombination centers.

ACKNOWLEDGMENTS

Sandia National Laboratories is a multiprogram laboratory managed and operated by Sandia Corporation, a wholly owned subsidiary of Lockheed Martin Corporation, for the U.S. Department of Energy's National Nuclear Security Administration under Contract No. DE-AC04-94AL85000. This research is funded by the U.S. government.

- [1] G. Lee, Y. Lo, Y. Lin, S. Bedair, and W. Laidig, Growth of InAs_{1-x}Sb_x ($0 < x < 1$) and InSb-InAsSb superlattices by molecular beam epitaxy, *Appl. Phys. Lett.* **47**, 1219 (1985).
- [2] D. Donetsky, S. P. Svensson, L. E. Vorobjev, and G. Belenky, Carrier lifetime measurements in short-period InAs/GaSb strained-layer superlattice structures, *Appl. Phys. Lett.* **95**, 212104 (2009).
- [3] B. C. Connelly, G. D. Metcalfe, H. Shen, and M. Wraback, Time-resolved photoluminescence study of carrier recombination and transport in type-II superlattice infrared detector materials, in *SPIE Defense, Security, and Sensing* (International Society for Optics and Photonics, 2013), p. 87040V.
- [4] B. Klein, N. Gautam, E. Plis, T. Schuler-Sandy, T. J. Rotter, S. Krishna, B. C. Connelly, G. D. Metcalfe, P. Shen, and M. Wraback, Carrier lifetime studies in midwave infrared type-II InAs/GaSb strained layer superlattice, *J. Vac. Sci. Technol. B* **32**, 02C101 (2014).
- [5] B. Olson, E. Shaner, J. Kim, J. Klem, S. Hawkins, M. Flatté, and T. Boggess, Identification of dominant recombination mechanisms in narrow-bandgap InAs/InAsSb type-II superlattices and InAsSb alloys, *Appl. Phys. Lett.* **103**, 052106 (2013).
- [6] Y. Aytac, B. Olson, J. Kim, E. Shaner, S. Hawkins, J. Klem, M. Flatté, and T. Boggess, Effects of layer thickness and alloy composition on carrier lifetimes in mid-wave infrared InAs/InAsSb superlattices, *Appl. Phys. Lett.* **105**, 022107 (2014).
- [7] E. Steenbergen, S. Elhamri, W. Mitchel, S. Mou, and G. Brown, Carrier transport properties of Be-doped InAs/InAsSb type-II infrared superlattices, *Appl. Phys. Lett.* **104**, 011104 (2014).
- [8] L. Höglund, D. Ting, A. Soibel, A. Fisher, A. Khoshakhlagh, C. Hill, S. Keo, and S. Gunapala, Minority carrier lifetime in mid-wavelength infrared InAs/InAsSb superlattices: Photon recycling and the role of radiative and Shockley-Read-Hall recombination mechanisms, *Appl. Phys. Lett.* **105**, 193510 (2014).
- [9] Y. Aytac, B. Olson, J. Kim, E. Shaner, S. Hawkins, J. Klem, M. Flatté, and T. Boggess, Temperature-dependent optical measurements of the dominant recombination mechanisms in InAs/InAsSb type-2 superlattices, *J. Appl. Phys.* **118**, 125701 (2015).
- [10] B. V. Olson, E. A. Kadlec, J. K. Kim, J. F. Klem, S. D. Hawkins, E. A. Shaner, and M. E. Flatté, Intensity- and Temperature-Dependent Carrier Recombination in InAs/InAs_{1-x}Sb_x Type-II Superlattices, *Phys. Rev. Applied* **3**, 044010 (2015).
- [11] H. Haugan, K. Mahalingam, F. Szmulowicz, and G. Brown, Quantitative study of the effect of deposition temperature on antimony incorporation in InAs/InAsSb superlattices, *J. Cryst. Growth* **436**, 134 (2016).
- [12] D. R. Rhiger, Performance comparison of long-wavelength infrared type II superlattice devices with HgCdTe, *J. Electron. Mater.* **40**, 1815 (2011).
- [13] B. V. Olson, E. A. Shaner, J. K. Kim, J. F. Klem, S. D. Hawkins, L. M. Murray, J. P. Prineas, M. E. Flatté, and T. F. Boggess, Time-resolved optical measurements of minority carrier recombination in a mid-wave infrared InAsSb alloy and InAs/InAsSb superlattice, *Appl. Phys. Lett.* **101**, 092109 (2012).
- [14] E. H. Steenbergen, B. C. Connelly, G. D. Metcalfe, H. Shen, M. Wraback, D. Lubyshev, J. M. Fastenau, A. W. K. Liu, S. Elhamri, O. O. Cellek, and Y.-H. Zhang, Significantly improved minority carrier lifetime observed in a long-wavelength infrared III-V type-II superlattice comprised of InAs/InAsSb, *Appl. Phys. Lett.* **99**, 251110 (2011).
- [15] B. Olson, C. Grein, J. Kim, E. Kadlec, J. Klem, S. Hawkins, and E. Shaner, Auger recombination in long-wave infrared InAs/InAsSb type-II superlattices, *Appl. Phys. Lett.* **107**, 261104 (2015).
- [16] C. Grein, M. Flatté, A. Evans, A. Hood, W. Tennant, and V. Nathan, *IEEE J. Sel. Top. Quantum Electron.* **19**, 1 (2013).
- [17] J. F. Klem, J. K. Kim, M. J. Cich, S. D. Hawkins, T. R. Fortune, and J. L. Rienstra, Comparison of nBn and nBp mid-wave barrier infrared photodetectors, in *OPTO* (International Society for Optics and Photonics, 2010), p. 76081P.
- [18] W. H. Lau, J. Olesberg, and M. E. Flatté, Electronic structures and electron spin decoherence in (001)-grown layered zincblende semiconductors, [arXiv:cond-mat/0406201](https://arxiv.org/abs/cond-mat/0406201).
- [19] J. Blakemore, *Semiconductor Statistics* (Dover Publications, Inc., Mineola, NY, 1962).
- [20] S. Rein, T. Rehr, W. Warta, and S. Glunz, Lifetime spectroscopy for defect characterization: Systematic analysis of the possibilities and restrictions, *J. Appl. Phys.* **91**, 2059 (2002).
- [21] M. E. Flatté and C. H. Grein, Ideal performance of and defect-assisted carrier recombination in MWIR and LWIR InAs/InAsSb superlattice detectors, in *SPIE OPTO* (International Society for Optics and Photonics, 2015), p. 93700K.
- [22] H. J. Haugan, G. J. Brown, S. Elhamri, S. Pacley, B. V. Olson, and T. F. Boggess, Post growth annealing study on long wavelength infrared InAs/GaSb superlattices, *J. Appl. Phys.* **111**, 053113 (2012).
- [23] R. N. Hall, Recombination processes in semiconductors, *Proc. IEEE* **106**, 923 (1959).
- [24] P. J. Lin-Chung and T. L. Reinecke, Theoretical study of native defects in III-V semiconductors, *Phys. Rev. B* **27**, 1101 (1983).
- [25] K. Alberi, J. Wu, W. Walukiewicz, K. M. Yu, O. D. Dubon, S. P. Watkins, C. X. Wang, X. Liu, Y.-J. Cho, and J. Furdyna, Valence-band anticrossing in mismatched III-V semiconductor alloys, *Phys. Rev. B* **75**, 045203 (2007).